Received: 9 May 2025 | Revised: 2 September 2025 | Accepted: 19 October 2025

DOI: 10.1002/qj.70067

Quarterly Journal of the Royal Meteorological Society RMetS

RESEARCH ARTICLE

The limits of knowing: An equilibrium between the observational gain and chaotic loss of information in data assimilation

Jie Feng[1,2] | **Zoltan Toth**[3] | **Malaquias Peña**[4]

[1]Department of Atmospheric and Oceanic Sciences and Institute of Atmospheric Sciences, Fudan University, Shanghai, China

[2]Shanghai Academy of Artificial Intelligence for Science, Shanghai, China

[3]Global Systems Laboratory, NOAA, Boulder, Colorado

[4]Department of Civil and Environmental Engineering, University of Connecticut, Storrs, Connecticut

Correspondence
Jie Feng, Department of Atmospheric and Oceanic Sciences and Institute of Atmospheric Sciences, Fudan University, Shanghai, China.
Email: fengjiefj@fudan.edu.cn

Funding information
National Natural Science Foundation of China, Grant/Award Number: 42375058

Abstract

Data assimilation (DA) is the most advanced tool for assessing the state of time-evolving chaotic systems. An estimate (analysis) is derived by combining information from the most recent and previous batches of observations, the latter of which are carried forward in time by first-guess (FG) forecasts started from previous analyses. Error variance in successful DA cycles fluctuates around an expected value. What factors determine this value? Three parameters are found to determine the level of analysis error variance (a^2) or the amount of information in state estimates: information extracted from the most recent set of observations by a DA system (I^o), the growth rate of error in FG (α), and the relative weight used for combining information from the latest observations and the FG (w). Our key recognition is that in DA systems with stationary performance, information gain from the most recent observations, and information loss due to chaotic error growth, in an expected sense, must be equal. Exploiting this equilibrium relationship, analysis error variance can be expressed as a function of the three driving parameters. Analysis information linearly and exponentially depends on I^o and α, respectively, while the optimal weight w is a simple function of the error growth rate. An evaluation of four operational DA systems from year 2008 reveals that their quality is driven by the amount of observational information they each extract from a virtually common set of globally available observations. The European Center for Medium-range Weather Forecast analysis demonstrates the lowest error variance among all evaluated operational systems. However, its analysis quality shows the least sensitivity to the tuning of weight w. The error equilibrium relationship reveals that a simple global adjustment of the relative weight between observations and FG may yield an up to 11%–43% reduction in error variance at the different centers.

KEYWORDS

cycled data assimilation, error equilibrium, observational information, state information

1 | INTRODUCTION

Observations are a cornerstone of natural sciences. In their totality, they are used to ascertain *general rule*s driving the dynamical behavior of systems, while its spatiotemporal subsets are used to estimate specific states of systems. Environmental monitoring (Kumar *et al.*, 2013), including data assimilation (DA; e.g., Ide *et al.*, 1997; Carrassi *et al.*, 2018) is a sophisticated implementation of state estimation. Under certain conditions, information about the state of a natural system extracted from observations may synchronize the behavior of an abstract replica (i.e., a numerical analysis) with its natural target (e.g., Bouttier & Courtier, 2002; Reichle, 2008; Zupanski *et al.*, 2007). The main question of this study is what controls the level of synchronization (i.e., the quality of analysis) if system dynamics is realistically captured in numerical models of a natural system (i.e., under perfect model assumptions).

Monitoring is used not only to track in real time, but by initializing forecasts, also to predict the future evolution of natural systems. Conceptually, science-based prediction of the state of natural systems consists of three main steps. First, using all available observations and related background knowledge, the dynamics of a system studied is captured in an abstract form (theory). Second, information about the state of the system is extracted from observations within a time window specific to that state (DA). And third, in the form of a numerical model, the system's dynamics is applied to the estimated state at one instant to carry information about the state forward in time (numerical modeling).

International agencies have been predicting the state of the atmosphere for decades now (Lazo *et al.*, 2009; Palmer, 2012; Schultz *et al.*, 2021). The skill of these forecasts has extended from days to up to two weeks (Zhang *et al.*, 2019). As attested by the stellar success of Numerical Weather Prediction (NWP; Simmons & Hollingsworth, 2002; Kalnay, 2003; Bauer *et al.*, 2015; Toth & Buizza, 2018), the evolution of synoptic-scale atmospheric processes can be well simulated with a discretized version of differential equations describing the spatiotemporal variation of atmospheric momentum and energy (Bechtold *et al.*, 2008; Charney *et al.*, 1950; Harris *et al.*, 2020; Richardson, 1922). Following Marshall and Molteni (1993) and others, for much of the discussion below we assume numerical models are near-perfect representations of the synoptic-scale component of atmospheric dynamics in the extratropics.

There exists a wide body of literature assessing different aspects of a variety of existing DA methods (Bannister, 2008; Hunt *et al.*, 2007; Lei & Whitaker, 2017; Wang *et al.*, 2013). Our study aims to identify the key parameters for the characterization of the equilibrium behavior of error and information (defined in Section 2) in DA cycles that produce skillful forecasts. What is the relationship in such equilibrated DA systems between information in the observations, the first guess (FG), and the analysis? And what factors control the quality of analysis states and ensuing forecasts?

The paper is organized as follows. Error and information as quality metrics of state estimates are introduced in Section 2. Numerical prediction and DA basics, and information and error in them are covered in Sections 3 and 4, respectively. A systematic, theoretical analysis of key natural and human factors controlling the basic behavior of error and information in DA cycles is presented in Section 5, while an application to operational weather forecast systems follows in Section 6. A discussion and some conclusions are offered in Section 7.

2 | ERROR AND INFORMATION

To ease discussions in the following sections, first we introduce two metrics we use for the evaluation of the quality of analysis and forecast products. Error is a commonly used, inverse metric of skill in analysis or forecast estimates of reality:

$$d'^2 = |\mathbf{G} - \mathbf{R}|^2, \tag{1}$$

where d'^2 is defined as the expected squared distance between an initial state (analysis) or forecast of a system ($\mathbf{G}$) and reality or a proxy of it ($\mathbf{R}$) represented on the same scales, and $|\cdot|$ represents the L_2 norm. Note that error in Equation (1) and elsewhere in the manuscript stands for "true" error, which is defined as the difference between an analysis or forecast and reality represented on the scales captured by the numerical fields (Peña & Toth, 2014). As reality is not known exactly, in the practical application of Section 6 we use the Statistical Analysis and Forecast Error (SAFE) algorithm to estimate true error in operational forecast systems (Feng *et al.*, 2023; Peña & Toth, 2014). For a more general definition that allows a comparison among different variables, error variance d'^2 can be standardized by the appropriate climatic variance of the variable in question (c^2):

$$d^2 = d'^2/c^2. \tag{2}$$

In the rest of this study we will use standardized expected error variance d^2 which is a dimensionless quantity with a range of 0 to 2 (see appendix C in Feng *et al.*, 2024).

Feng *et al.* (2024) introduced an alternative metric for assessing the performance of analysis and forecast systems at a given spatial resolution. Information (I) in an analysis or forecast equals the orthogonal projection of its anomaly onto the anomaly of reality, both anomalies taken from the climatic mean and standardized by the climatic variance:

$$I = \frac{|\mathbf{G}-\mathbf{C}|^2}{|\mathbf{R}-\mathbf{C}|^2}\cdot r^2 = \frac{|\mathbf{G}_\mathrm{p}-\mathbf{C}|^2}{|\mathbf{R}-\mathbf{C}|^2}, \tag{3a}$$

where $\mathbf{G}-\mathbf{C}$ and $\mathbf{R}-\mathbf{C}$ represent anomaly fields of analysis or forecast $\mathbf{G}$ and reality $\mathbf{R}$ on the same grid from the climatic mean $\mathbf{C}$, respectively, and $\mathbf{G}_\mathrm{p}$ is the orthogonal projection of $\mathbf{G}$ onto the anomaly of reality (i.e., $\mathbf{R}-\mathbf{C}$). r represents the correlation coefficient between the anomalies of $\mathbf{G}$ and $\mathbf{R}$, or the anomaly correlation coefficient (ACC) between forecasts and reality. Correspondingly, information is a measure of statistical resolution or forecast skill, one of two major performance attributes (Toth *et al.*, 2006), and it varies between 1 and 0 (perfect or no knowledge about the state of a natural system, respectively).

The rest of the anomaly variance in numerical analyses or forecasts $\mathbf{G}$, termed as Noise (N), is unrelated to reality and hence orthogonal to information I:

$$N = \frac{|\mathbf{G}-\mathbf{C}|^2}{|\mathbf{R}-\mathbf{C}|^2}\cdot\left(1-r^2\right) = \frac{|\mathbf{G}-\mathbf{G}_\mathrm{p}|^2}{|\mathbf{R}-\mathbf{C}|^2}. \tag{3b}$$

Let us denote the anomaly variance of forecast or analysis and reality as g^2 and c^2, respectively, that is, $|\mathbf{G}-\mathbf{C}|^2 = g^2$ and $|\mathbf{R}-\mathbf{C}|^2 = c^2$. On scales well resolved, numerical models are assumed to have a realistic level of variance (i.e., $g^2 = c^2$). Conveniently, the sum of information and noise variances in such systems equals 1:

$$I + N = 1. \tag{4a}$$

In this situation, information as defined here equals the variance of the standardized observed anomaly explained by the standardized analysis or forecast anomaly, which is the square of the commonly used ACC (Feng *et al.*, 2024):

$$I = r^2. \tag{4b}$$

For systems with a realistic level of variance, error variance (d^2) standardized by the climatic variance and I also have a relatively simple relationship (Feng *et al.*, 2024):

$$d^2 = 2\cdot\left(1-\sqrt{I}\right), \tag{5a}$$

and

$$I = \left(1-\frac{1}{2}d^2\right)^2. \tag{5b}$$

For forecast systems with realistic variance, information and error variance therefore are interchangeable, positively and negatively oriented metrics for assessing the quality of state estimates (i.e., analysis or forecast), respectively. From here on we assume that the variance in analysis and forecast anomalies matches that in reality, which to a good extent is satisfied for 500-hPa height forecasts (Peña & Toth, 2014) studied in Section 6. In the rest of this study, information and error variance will then be used as alternative metrics of analysis and forecast performance.

3 | NUMERICAL PREDICTION

Numerical prediction is a sophisticated procedure to estimate future states of nature through observing system measurements, numerical modeling, and data assimilation. Among these components, DA plays a pivotal role by providing initial conditions for accurate numerical forecasts. This section offers a concise overview of the observing and numerical modeling systems, followed by a detailed explanation of the key procedures involved in DA.

3.1 | Observations

Real-world atmospheric measurements from an array of in situ and remote observing systems are taken either randomly or on a schedule both in time and space (left side of Figure 1). Observations are affected by measurement errors but each may contain some unique information about the state of the atmosphere. These observation data are integrated with numerical models through the DA system to reduce errors in the analysis of the natural state (Bouttier & Courtier, 2002).

3.2 | Numerical modeling

Numerical models replicate the deterministic dynamics[i] of the resolved-scale component of the atmosphere in an abstract setting (middle part of Figure 1). In that space, prognostic variables on a discretized grid approximate the resolved-scale atmospheric conditions of the real atmosphere. An application of numerical models to an estimate of the state of the system at any point in time then dynamically projects the initial condition into the future. The inverse of observation operators (see next subsection) or other interpretation relate, or bring back the abstract forecast process to the perceptible world in the form of observable quantities or weather conditions (Albers *et al.*, 2020) that may affect socioeconomic activities (right side of Figure 1).

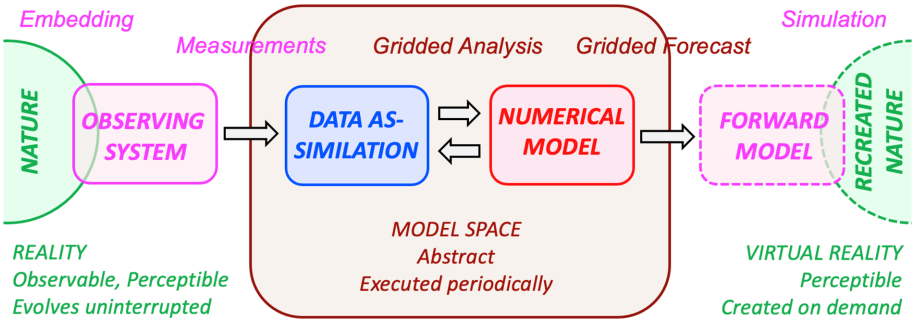

FIGURE 1 Schematic diagram of the coupled Nature, Observing, Data Assimilation, and Prediction systems. For further details, see text.

The global atmosphere is often considered as a complex, multiscale chaotic (i.e., aperiodic) nonlinear dynamical system (Charney, 1948; Li *et al.*, 2006; Lorenz, 1969; Sun & Zhang, 2016). It is well understood that in such systems with increasing lead time forecast skill or information is gradually lost. Eventually, barring any bias, forecast error variance (d^2) asymptotes to a level twice the climatic variance of a system (i.e., $2c^2$; Leith, 1974; Kalnay, 2003; Li *et al.*, 2018). At that point forecasts become indistinguishable from randomly chosen states of the system, hence all information about the specific state of a natural system is lost (i.e., $I = 0$; Li & Ding, 2011; Feng *et al.*, 2019).

3.3 | Data assimilation

Data assimilation techniques integrate information from current and past observations into what is called an analysis or initial condition, in the form of model prognostic variables. Though DA uses various methodologies – such as the sequential assimilation of observations in the ensemble Kalman filter, or simultaneous assimilation in the variational framework (see, e.g., Lorenc, 2003) – these approaches share a common underlying conceptual design.

Step 1. Even in the absence of any new observation, a forecast carries information obtained from past observations to future times. Though information about the state of a system is lost with increasing lead time, a numerical forecast (**F**) started from the previous analysis (often called a first guess (FG), the prior, or background field) is a key element in data assimilation. FG forecasts capture information that was extracted from all past observations, parts of which is retained in a sequence of "cycled" FG forecasts.

Step 2. Next, if available, DA systems extract new (i.e., additional to what is already contained in the FG) information about the state of a natural system from observations collected over a relatively short recent period of time called assimilation window. This is done via observation operators that relate atmospheric and other measurements to the abstract space of model prognostic variables directly affected by the measurements, as differences or "observation increments" from the FG. In practice, observations taken in an assimilation window offer an incomplete description of the state of the system.

Step 3. Using dynamical connections among model variables in the form of a background error covariance matrix (Bannister, 2008; Wang *et al.*, 2008a; Wang *et al.*, 2008b), DA systems propagate in time and space the incomplete observational data available from model variables that are directly related to the new measurements to all those variables at analysis time that are not. Though not accessible explicitly, this amounts to a hypothetical *observational field* (**O**), the anomaly of which from the climatic mean reflects the effect of observations taken in the assimilation window only.

Step 4. Finally, DA systems combine the FG forecast (Step 1) and the newly available observational field **O** (Step 3) in a new analysis (**A**, a posterior estimate), a numerical replica of the natural system at analysis time.

Conceptually, an analysis (**A**) can be considered as a weighted sum of the FG **F** that carries information from the past, and the hypothetical observational field **O** that reflects observational information extracted from the latest set of observations, respectively (Bannister, 2017; Lorenc, 1986):

$$\mathbf{A} = w\mathbf{F} + (1 - w)\mathbf{O}, \tag{6}$$

where w is a scalar weighting factor on the FG, reflecting the ratio between error variances assumed in the FG and observational fields (varying between 0 and 1).[ii] Typically, $w > 0.5$ as the FG **F** is assumed to contain more information from past observations than **O** based only on recently collected observations (see Section 6.3 and Bouttier & Courtier, 2002).

Equation (6) amounts to a Bayesian, observationally based update of the prior (i.e., the FG; Daley, 1991; Courtier *et al.*, 1994; Ide *et al.*, 1997). In practice, DA systems are executed in the form of a recursive two-part cycle (Bertino *et al.*, 2003). Part or phase one is a short-range (usually six hours or shorter) model forecast initialized

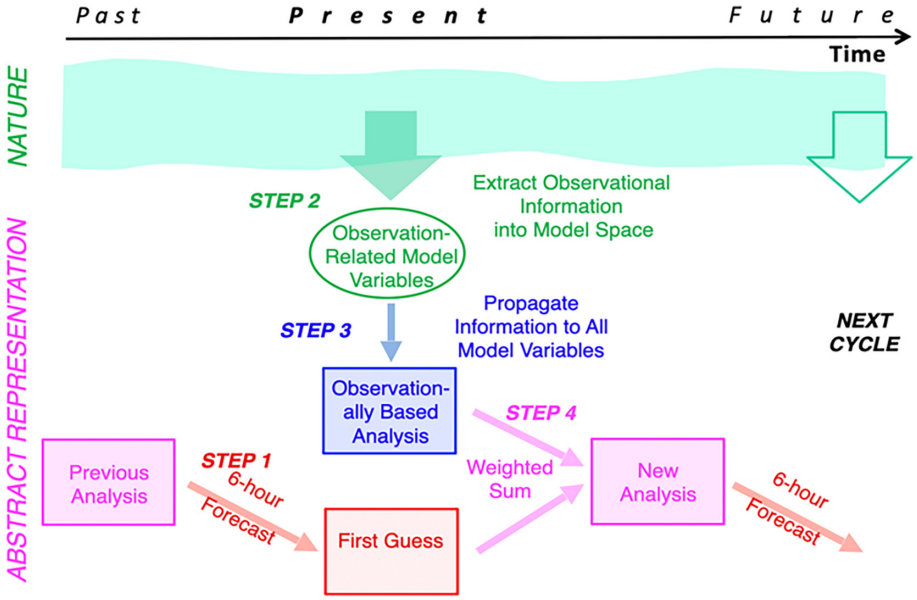

FIGURE 2 Schematic of the four steps in data assimilation. For details, see text.

from the previous analysis (Step 1 above), while the second, observational update part comprises Steps 2–4 above (Figure 2).

4 | ERROR AND INFORMATION IN DATA ASSIMILATION CYCLES

In this section we review the sources and types of error in analysis and FG forecasts, and their relationship with observational error.

4.1 | Sources of error

As discussed in Section 2, information (Equation 3a) and error variance (Equation 2) are alternative measures of the quality of state estimates (Equation 6). The sources of error, or of incomplete information in the analysis are multitude and include, first, the loss of information carried forward in a FG forecast from a previous analysis due to chaotic dynamics (Step 1 in Section 3.3). Second, observations are burdened with measurement error (Section 3.1; Cao *et al.*, 2007). Third, model variables like gridpoint or gridbox temperature that comprise the initial condition are not observable in nature and their relationships with observed quantities are only approximated, leading to representativeness and observation operator-related errors (Step 2, Janjić *et al.*, 2018). Fourth, background error covariances used to propagate information in certain model variables extracted from available observations to different model variables at other locales and times offer only estimates of dynamical relationships that exist in nature (Step 3, Bannister, 2008; Wang *et al.*, 2008a, Wang *et al.*, 2008b). Fifth, estimated error variances for observations and the FG used in their combination in Step 4 of DA are inaccurate (Section 4.5). Sixth and most importantly, given limitations in the type and quantity of observations, and also in the various assimilation techniques mentioned above, the level of information about the state of the system that can be captured in an analysis is limited.

4.2 | Types of error

4.2.1 | Error in position

As discussed by Feng *et al.* (2024), due to the statistical nature of DA, analysis states necessarily lie off the model's trajectory. During a transitionary period (Section 4.2.2), the stable part of model dynamics removes any imbalances from initial states which makes the evolving state asymptote the model's trajectory. Due to errors, or limited observational information in the initial condition (i.e., analysis), the forecast, however, is not landing on the segment of the model trajectory exactly representing the resolved component of reality. Instead, it lands on another segment of the trajectory that is nearby in phase space (but distant in time along the trajectory). At that point, information and noise in a forecast reflect what is common and different, respectively, between reality and its representation on the model's trajectory.

We call the difference between reality and our estimate of reality on the model's trajectory the *error in the position of the analysis*. By position we refer to the specific locations of the states of reality and its estimate *on the model's trajectory*. Driven by the unstable part of model dynamics (Kalnay, 2003; Patil *et al.*, 2001), until nonlinearities

become dominant, the two ensuing segments of a chaotic system's trajectory diverge. Just as true forecast error (i.e., difference between a forecast and reality on the model's grid), the difference between the two, initially close, segments of the model's trajectory grow exponentially (Lorenz, 1963):

$$f_u^2 = a_u^2 \cdot e^{\alpha \cdot \Delta t}, \tag{7}$$

where a_u^2 and f_u^2 are standardized analysis and forecast error variances with respect to reality in the unstable subspace, α (α>0) is the exponential growth rate, and Δt is the length of the assimilation cycle. This type of error in an analysis or forecast is dynamically conditioned and reside in a narrow, unstable subspace of the system's dynamics, reflecting the natural variability of the system.

4.2.2 | Off-trajectory error

In contrast, the rest of the error, which places the initial condition off a system's trajectory (i.e., into a space that the state of a system never visits naturally), is dynamically unconditioned (see section 4.3.3 in Feng *et al.*, 2024). These random errors span a much wider, stable subspace (Tondeur *et al.*, 2020) with neutral or decaying components. As indicated above, when a model's dynamics is applied, over a transitionary period, random errors are reduced, making the evolving state quickly asymptote the closest segment on a model's trajectory. Following Feng *et al.* (2020), analysis error variance from this stable subspace (a_s^2) is assumed to shrink at an exponential rate of β ($\beta < 0$), to become the random error in the first guess, denoted by f_s^2:

$$f_s^2 = a_s^2 \cdot e^{\beta \cdot \Delta t} \tag{8}$$

All sources of error listed in Section 4.1 contribute to both types of error, except the dynamical loss of information (Source 1) affects only positional, but not off-trajectory errors.

4.3 | Total error

Since positional (growing) and off-trajectory (decaying) errors are governed by different parts of a system's dynamics (the unstable and stable manifolds, respectively), these errors are orthogonal to each other and can be handled separately (see Equations 7 and 8). Total analysis and forecast error variances (i.e., a^2 and f^2) are hence the sum of their growing and decaying components:

$$a^2 = a_u^2 + a_s^2 \tag{9a}$$

$$f^2 = f_u^2 + f_s^2 \tag{9b}$$

Toth and Kalnay (1997) suggested that due to the cyclic use of short-range forecasts, a significant part of analysis error must be dynamically conditioned and exponentially growing. Feng *et al.* (2020) found that the proportion of decaying errors in the analysis error of the NCEP DA system is indeed relatively small; for both wind and temperature, it is only about 5% of the total analysis error variance. And since the application of system dynamics diminishes the decaying component of error, the proportion of growing, dynamically conditioned error in free forecasts further increases as a function of lead time (see, e.g., Figure 4 of Feng *et al.*, 2020 and Hamill *et al.*, 2002). Beyond a short transitionary period, total error therefore can be approximated with its growing component. For most of the discussion below decaying error is therefore ignored and growing error is considered as a proxy for total error. Note that since decaying errors reflect off-trajectory behavior, and since information, by definition reflects only the natural dynamics of a system, the relationships between error and information captured in Equations (5a) and (5b) strictly are valid only in the growing subspace.

4.4 | Relationship between background, observational, and analysis error

Here we attempt to establish the relationship between error variances in the background, observational, and analysis fields. Subtracting reality (**R**) from the analysis (**A**), FG forecast (**F**), and the observational (**O**) fields in Equation (6), true error in the analysis can be written as:

$$\mathbf{A} - \mathbf{R} = w(\mathbf{F} - \mathbf{R}) + (1 - w)(\mathbf{O} - \mathbf{R}). \tag{10}$$

Error in the hypothetical observational field is a function of the latest set of observations, which are independent of error sources in the FG. As such, observational (**O**) and FG (**F**) errors can be considered as random draws from the space of error in state estimates. Since this space is high-dimensional (Feng *et al.*, 2024), following the Curse of Dimensionality (Bengtsson *et al.*, 2008) we assume that $\mathbf{F} - \mathbf{R}$ and $\mathbf{O} - \mathbf{R}$ are orthogonal. **O**, **F**, **A** and their distance from, or their expected error with respect to reality **R** (o, f, and a, respectively) is then represented with the right-angle triangle in Figure 3.[iii]

4.5 | Optimal weight and optimal analysis

Considering Equation (10) and exploiting the orthogonality assumption, analysis error variance a^2 can be expressed as a weighted sum of background error variance f^2 and

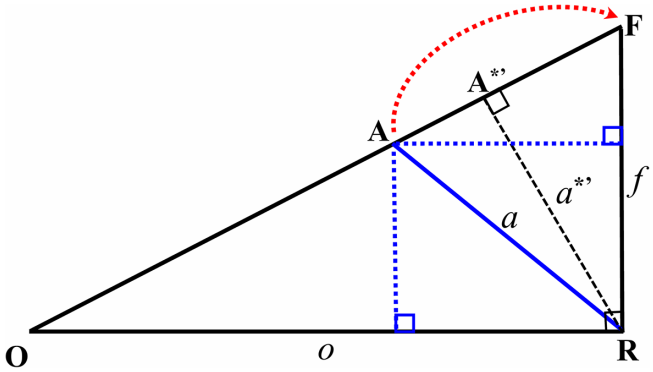

FIGURE 3 Schematic of the position of the actual analysis (**A**), first guess (**F**), hypothetical observation (**O**), and the analysis field with an optimal weight (**A**$^{*\prime}$) in the model's space, positioned at a, f, o, and $a^{*\prime}$ distance from reality (**R**). Error in the observational update and forecast phases of DA are highlighted in blue and red, respectively. Error in the analysis with an optimal weight is shown as a dashed black line. For further details, see text.

observational error variance o^2:

$$a^2 = w^2 f^2 + (1-w)^2 o^2. \tag{11}$$

Hereafter, Equation (11) is called the generalized analysis precision equation (G-APE). To minimize analysis error, according to the least-squared method, the ratio of the optimal weights on the first guess (w^* in *Step 4*, Section 3.3, Equation 6) and on the observational field ($1-w^*$) must be equal to the ratio of true error variances in the observational and background fields (Bouttier & Courtier, 2002; Kalnay, 2003):

$$w^*/(1-w^*) = o^2/f^2, \tag{12a}$$

from which the optimal weight on the first guess (FG) is:

$$w^* = o^2/\left(f^2+o^2\right). \tag{12b}$$

Given information present in **F** and accessed from the latest set of observations **O**, the analysis state corresponding to the optimal weight w^* in Figure 3 is denoted by **A**$^{*\prime}$. The lowest analysis error $a^{*\prime}$ in a given cycle with FG and observational errors of f and o, respectively can be expressed in an inverse form (Bouttier & Courtier, 2002; Kalnay, 2003) via the combination of Equations (12b) and (11):

$$\frac{1}{a^{*\prime 2}} = \frac{1}{f^2} + \frac{1}{o^2}. \tag{13}$$

Equation (13) we call the optimal analysis precision equation (O-APE).

Interestingly, combining Equations (7), (12b), and (13) we find that w^*, the weight on the FG that leads to the optimal analysis is independent of the observational information, and depends only on the growth rate of error:

$$w^* = 1/\mathrm{e}^{\alpha\cdot\Delta t}, \tag{14}$$

from which, with basic algebra, we arrive at the following simple relationship for the optimal ratio of weights on **F** and **O**:

$$w^*/(1-w^*) = o^2/f^2 = 1/\left(\mathrm{e}^{\alpha\cdot\Delta t}-1\right). \tag{15}$$

Equations (14) and (15) offer a general solution for optimal weights on the FG and observations.

Up until now the optimal background and observational error variances or their ratio have been unknown. Since their estimation has been considered challenging and related results unsatisfying (Bouttier & Courtier, 2002; Janjić *et al.*, 2018), in practical applications the weight factor w^{iv} is generally different from its ideal value w^*. This yields an analysis (**A**) with an error larger than that in an analysis made with optimal weights (**A**$^{*\prime}$).

Note that **A**$^{*\prime}$ denotes an analysis from a single application of w^*, given f and o. As shown in Section 5.5, with the repeated application of the same weight, analysis error after a transitionary period equilibrates. What is the equilibrated error variance in an analysis (**A***) using the optimal weight (w^*)? Considering that analysis and forecast errors are linked by the growth of error, the equilibrated or time mean error in an analysis using the optimal weight w^* can be quantified with the combination of Equations (7) and (13):

$$a^{*2} = \left(1-\mathrm{e}^{-\alpha\cdot\Delta t}\right)\cdot o^2. \tag{16}$$

Equation (16) shows that equilibrated error variance in the optimal analysis **A*** depends only on a natural and on a forecast system parameter, the rate of divergence of initially close segments of the trajectory of nature (or the growth of error in a forecast made with a perfect model, α), and the level of observational information used in the analysis (or its inverse, observational error variance o^2), respectively.

5 | EQUILIBRIUM BEHAVIOR

This study is based on the observation that in successful DA applications, after an initial adjustment period, the total analysis error variance stabilizes at a level significantly below the "no skill" benchmark (defined as twice the climatic variance). This is evident from the long-term performance statistics of international NWP

centers (De Rosnay *et al.*, 2022; Raynaud *et al.*, 2011; Wang *et al.*, 2024). Apart from some variations caused by seasonal and regime-dependent fluctuations in error growth, the analysis fields in these successful systems consistently track (i.e., do not diverge from) the real state of the atmosphere. Error in analysis fields of well performing systems remains statistically stationary over time (see also Section 5.5).

As growing and decaying errors evolve in the mutually independent unstable and stable subspaces, quasistationarity holds for both. Below we unfold the main thesis of this study about the equilibrium between the observational gain and the forecast loss of information in DA systems that track reality.

5.1 | Stable subspace

A quasistationary level of decaying analysis error variance implies an equivalence between the addition of random noise in the observational update part (Section 3.1), and the reduction of random noise in the forecast part of DA (Equation 8). The associated equilibrium in the stable subspace is evident from a rearrangement of Equation (11):

$$a_s^2 - w^2 \cdot f_s^2 = (1-w)^2 \cdot o_s^2, \tag{17}$$

where subscript s indicates error components in the stable (decaying) subspace. Equation (17) implies that random error variance added into the analysis with the assimilation of observations (rhs of Equation 17) equals the reduction of random error variance from the decay of such errors in the FG that were added into the analysis (lhs of Equation 17). A combination of Equations (8) and (17) reveals that decaying error in the analysis (a_s^2) can be written as a function of decaying error in the observational field (o_s^2), the decay rate of such errors (β), and the weighting factor used in Step 4 of DA (w):

$$a_s^2 = (1-w)^2 \cdot o_s^2 / \left(1 - w^2 \cdot e^{\beta \cdot \Delta t}\right). \tag{18}$$

5.2 | Unstable subspace

Similarly, stationary behavior indicates an equivalence in the unstable subspace between the reduction of error in the observational update, and an increase of error in the forecast parts of DA (Crisan & Ghil, 2023). An equilibrium between the growth of error in the FG and the reduction of growing error in the observational update part of the analysis is evident from a rearrangement of Equation (11) in the unstable subspace:

$$w^2 \cdot f_u^2 - a_u^2 = -(1-w)^2 \cdot o_u^2. \tag{19}$$

Equation (19) indicates that the addition of growing error from the FG into the analysis (lhs Equation 19) equals the reduction of analysis error variance due to the use of the observational field (rhs Equation 19). Combining Equations (7) and (19), analysis error in the unstable subspace can be written as a function of growing error in the observational field and its growth rate:

$$a_u^2 = (1-w)^2 \cdot o_u^2 / \left(1 - w^2 \cdot e^{\alpha \cdot \Delta t}\right). \tag{20}$$

The five parameters that under general conditions describe the behavior of error in the unstable and stable subspaces in DA cycles are listed in Table 1. Since decaying errors are small and affect only very short-range forecasts (Section 4.3), in the rest of this study we use growing error variance discussed above, and information introduced below, both defined in the unstable subspace as alternative metrics to study the performance of DA systems.

5.3 | Information in the analysis

For simplicity of notation, we introduce $F(I)$ as a continuous and monotonic function of information I:

$$F(I) = 1/(2 \cdot (1 - \sqrt{I})) = 1/d^2. \tag{21}$$

TABLE 1 Key parameters used for assessing the behavior of information and error in data assimilation cycles, as well as the subspaces of dynamics they are affected by, and the systems they reflect. For further details, see text.

Parameter	Symbol	Description	Subspace	System
Observational error variance	o_u^2	Growing error in latest set of observations	Unstable	Observing and data assimilation
Exponential growth factor	α	Divergence of trajectory segments		Nature
Weight factor	w	Controls how much extracted observational information is used		Data assimilation
Random noise	o_s^2	Decaying error in observations	Stable	Observing and Data assimilation
Exponential decay rate	β	Convergence to model trajectory		Nature

As such, in the rest of this study we will use $F(I)$ as an alternative measure of information. As seen from th right-hand side of Equation (21), $F(I)$ equals the inverse of error variance, also offering an alternative measure for the accuracy of the state estimate. Combining Equations (21) and (7) reveals how initial information (I^{a}) is reduced as a function of forecast lead time (I^{f}):

$$F\left(I^{\mathrm{f}}\right) = F\left(I^{\mathrm{a}}\right) \cdot \mathrm{e}^{-\alpha \cdot \Delta t}. \tag{22}$$

Considering Equation (20), the level of information in the analysis can then be expressed as:

$$F\left(I^{\mathrm{a}}\right) = \left(1 - w^2 \cdot \mathrm{e}^{\alpha \cdot \Delta t}\right) \cdot F\left(I^{\mathrm{o}}\right)/(1-w)^2. \tag{23}$$

Equation (23) is a key result of our study, indicating that the equilibrium level of information in the analysis (I^{a}) is a function of the dynamics of the atmosphere (error growth α), information extracted by Steps 2–3 of the DA system from the latest set of observations (I^{o}), and the efficiency at which this information is used in Step 4 of the data assimilation system in preparing the analysis (weighting factor w). For an analysis made with the optimal weight w^* (Equation 14), Equation (23) simplifies to:

$$F\left(I^{\mathrm{a}*}\right) = F\left(I^{\mathrm{o}}\right)/\left(1 - \mathrm{e}^{-\alpha \cdot \Delta t}\right). \tag{24}$$

Equation (24) indicates that information, just as error (Equation 16) in an analysis with optimal weights depends only on two factors: information accessed from the latest set of observations, and the divergence rate between initially close segments of the system's trajectory.

Since the observational field **O** is defined as an increment from the FG forecast field **F**, just as error (Section 3.3, Step 3, and Section 4.4), information in **O** and **F** are independent. According to Equation (13), information in the analysis ($F(I^{\mathrm{a}*})$) with optimal weight w^* can hence be written as the sum of information in the FG ($F\left(I^{\mathrm{f}}\right)$) and observational fields ($F(I^{\mathrm{o}})$):

$$F\left(I^{\mathrm{a}*}\right) = F\left(I^{\mathrm{f}}\right) + F\left(I^{\mathrm{o}}\right), \tag{25}$$

from which it follows that information gain in the observational update ($F(I^{\mathrm{o}})$), and information loss in the forecast part of equilibrated DA systems ($F(I^{\mathrm{a}*}) - F\left(I^{\mathrm{f}}\right)$) must be equal.

5.4 | The influence of past observations

Ultimately, all analysis information, including what is carried forward by the recursive use of FG forecasts originates from observations taken over the current and preceding DA cycles. What is the contribution of observations from each assimilation cycle in the past? To quantify the effect of past observations, we first consider that information in an FG can be expressed as a function of analysis information and error growth rate (Equation 22). Information (i.e., $F\left(I^{\mathrm{a}*}_{-i}\right)$) in an analysis i cycles before current time ($t = 0$) can then be written as the sum of information in the FG and in the latest batch of observations at that time:

$$F\left(I^{\mathrm{a}*}_{-i}\right) = F\left(I^{\mathrm{f}}_{-i}\right) + F\left(I^{\mathrm{o}}_{-i}\right) = \mathrm{e}^{-\alpha_{-i} \cdot \Delta t} \cdot F\left(I^{\mathrm{a}*}_{-i-1}\right) + F\left(I^{\mathrm{o}}_{-i}\right). \tag{26}$$

For simplicity, we assume that both observational information and error growth rate are stationary in time. In light of the exponential growth of error and the recursive nature of data assimilation and by iteratively using Equation (26), information in the latest analysis ($t = 0$) can then be expressed as a weighted sum of observational information used in the current and all prior cycles:

$$F\left(I^{\mathrm{a}*}\right) = F\left(I^{\mathrm{o}}\right) + \sum_{i=1}^{+\infty} \mathrm{e}^{-i \cdot \alpha \cdot \Delta t} F\left(I^{\mathrm{o}}\right). \tag{27}$$

Equation (27) quantifies the contribution of observations from all past cycles to information in the latest analysis, reflecting the decay of information in each FG forecast due to the exponential growth of error in chaotic systems.

As an example, Figure 4 displays observational information in the latest European Center for Medium-range

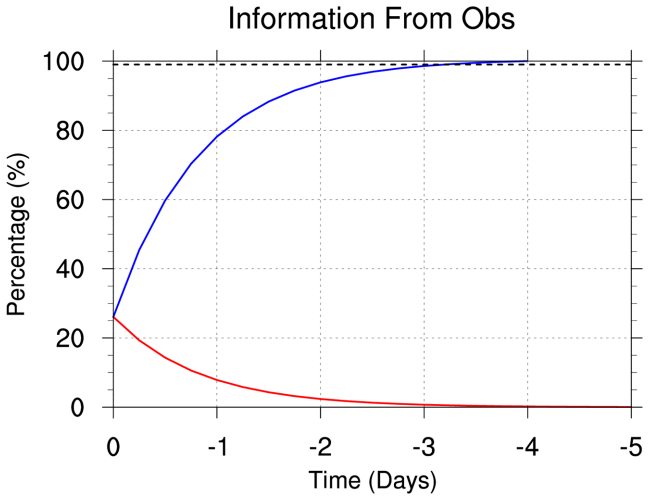

FIGURE 4 Information in European Center for Medium-range Weather Forecast (ECMWF) analysis fields of 500-hPa geopotential height (characterized by $a^{*2} = 6.6\ \mathrm{m}^2$, $o^2 = 25.3\ \mathrm{m}^2$, and $\mathrm{e}^{\alpha \cdot \Delta t} = 1.35$, see Table 2) derived from past observations taken at individual times (red line), or accumulated back to specific times (blue line). The horizontal black dashed line denotes $I = 0.99$.

TABLE 2 Estimates for seven parameters of the four operational DA systems studied. For further details, see text.

Parameter/ center	Analysis error variance	Exponential growth rate	Weight on first guess	Optimal weight on first guess	First-guess error	Observational field error variance	Optimal analysis error variance
Symbol	a^2 (m^2)	$e^{\alpha \cdot \Delta t}$ (/6 hours)	w	w^*	f^2 (m^2)	o^2 (m^2)	a^{*2} (m^2)
NCEP	38.0	1.28	0.66	0.78	48.6	146.3	32.0
CMC	29.5	1.31	0.60	0.76	38.6	98.0	23.2
ECMWF	11.5	1.35	0.40	0.74	15.5	25.3	6.6
FNMOC	49.2	1.30	0.68	0.77	64.0	190.0	43.8

Weather Forecast (ECMWF) analysis originating from past single (red line), or cumulatively from the most recent analysis times (blue line). The calculation of the contribution of observational information follows Equation (27) using the parameters offered in Table 2. According to Figure 4, the latest set of observations contribute only 27% of the total information in the analysis (red line at $t = 0$), with the rest coming from the FG. This is consistent with the general DA practice of assigning smaller error variance to the FG than to individual observations, and the widely held belief that the FG is more informative about the state being estimated than the entire collection of the latest batch of observations (Bouttier & Courtier, 2002).

Pires *et al.* (1996) recognized that the length of what they called the "efficient assimilation period" depends on the rate of error growth, and offered seven days as a "crude estimate" of its length. Given the average error growth rate we find that most (99%) effect from past observations is from the most recent 72-hour period (see blue curve in Figure 4). This period is up to six times longer than the current time window used in the operational 4DVar DA system at ECMWF (12 hours, Bouttier, 2001). The results in Figure 4 suggest that if challenges related to nonlinearities could be overcome, an extension of the 12-hour window used in today's operations may be beneficial. With longer time windows, analysis quality would likely benefit from a more optimal use of observational data.

5.5 | Transitional behavior and filter divergence

So far we have considered the long-term expected behavior of relatively small, exponentially growing errors (Equations 20 and 16) and related information (Equations 23 and 24) with non-optimal and optimal analysis weights, respectively. When an analysis cycle is started for the very first time, if the prevailing error growth rate and available observational information allows for the successful tracking of the state of reality, the equilibrium analysis error level is approached over a transitional period. The time it takes for error variance in an analysis cycle started for the first time with an FG of a specific quality to asymptote to its expected value is investigated, still in an expected sense, in Appendix A.

In real life, both error growth rate and observational information fluctuate around their expected values. In practical DA applications, this results in cycle-to-cycle variations in error variance. If in any cycle analysis information (due to fast error growth and/or low observational information) becomes too low, shadowing reality cannot be maintained. This behavior, referred to as "filter divergence" (Anderson, 2001) happens if observational information available in any cycle is lower than the loss of information due to error growth in that cycle. Filter divergence can be avoided only if DA can extract enough information from existing, or from additional independent observations to overcome the chaotic loss of information in the FG.

6 | QUANTITATIVE ASSESSMENT

By applying the analysis equilibrium relationships captured in Equations (16), (20), (23), and (24), in this section we first investigate how the expected or time average quality of the analysis (measured by error variance or information in the analysis) depends on the level of error growth, observational information, and the weight used for the combination of information from the FG and the latest set of observations. The behavior of typical operational DA systems will then be assessed and interpreted in the context of the simulated results.

6.1 | Simulation

6.1.1 | Analysis quality with optimal weight

As seen from Equations (16) and (24), error variance (a^{*2}) and information (I^{a*}) in an analysis made with optimal weights (Equation 14) are both a linear function of error

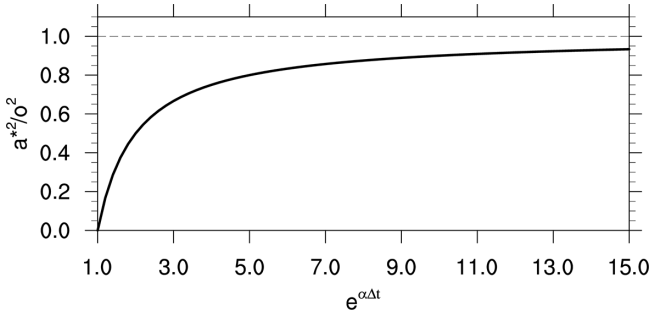

FIGURE 5 The ratio between a^{*2} and o^2 (i.e., $1 - e^{-\alpha \cdot \Delta t}$, see Equation 16) as a function of the error growth rate. For further details, see text.

variance in the observational field (o^2), and an exponential function of the dynamical error growth rate ($e^{\alpha \cdot \Delta t}$). The latter, exponential behavior is highlighted in Figure 5. Plotted there is the ratio of error variances in the analysis versus the observational fields, as a function of growth rate. The larger this ratio, the smaller weight is exerted on the FG in the analysis. With increasing growth rate the ratio increases and asymptotes to 1, indicating that the positive effect of cycling information in DA is less pronounced when the growth rates are high. Evidently, more unstable dynamics diminishes the effect of past observations, hence error variance (and information) in the analysis becomes indistinguishable from that in the latest set of observations.

The combined effect of observational error variance and error growth rate on the quality of analyses with optimal weights (Equation 16) is illustrated in Figure 6. Interestingly, either complete observational information ($I^o = 1$ or $o^2 = 0$), or stable dynamics ($\alpha = 0$) ensures a perfect analysis ($I^{a*} = 1$), irrespective of the other driving factor. When either of the two factors is near ideal, analysis information is relatively insensitive to the value of the other factor and remains near optimal. This is due to the minimal loss of information in an FG when the error growth rate is very low, and the dominance of observational information, when it is high, no matter how fast information is lost in the FG.

With Figure 6, one can explore how more or higher-quality observations, or higher error growth rates affect the quality of analyses. Such an evaluation can complement results from actual (OSEs, Wang *et al.*, 2008a, Wang *et al.*, 2008b) or simulated observing system experiments (OSSEs, Privé & Errico, 2013), which are generally rather expensive. An example is the geographical distribution of analysis and forecast error variance in the extratropics. Upper-level extratropical jets are known to exhibit stronger baroclinic instabilities compared to circulation at lower levels, responsible for higher error growth rates (Holton & Hakim, 2012). Assuming observational

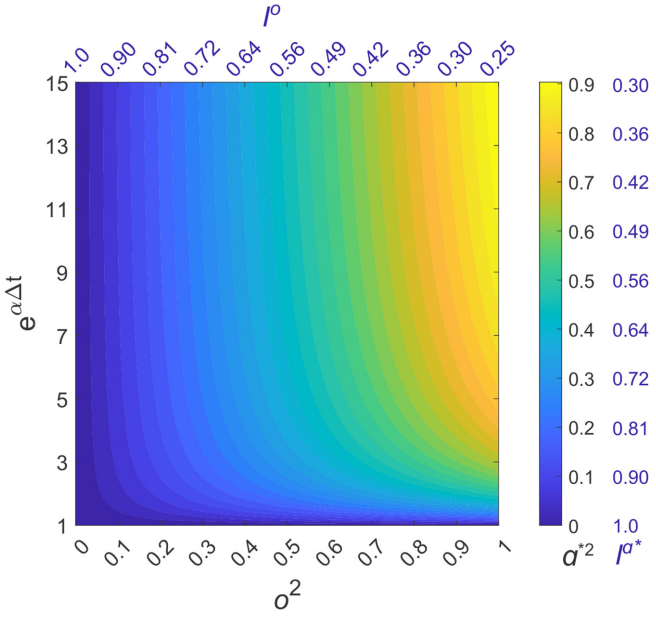

FIGURE 6 Standardized analysis error variance a^{*2} and analysis information (I^{a*}) as a function of standardized observational error variance o^2 and error growth rate $e^{\alpha \cdot \Delta t}$ based on Equations (16) and (24).

information is uniformly distributed, Figure 6 can be used to assess analysis error variance as a function of height and geographical location. Specifically, Figure 6 suggests that true forecast and analysis error variances for wind are greater at the height of the upper-level jet (250–300 hPa) than in the rest of the troposphere, consistent with the findings of Feng *et al.* (2020) and Wang *et al.* (2013).

6.1.2 | The effect of sub-optimal weights

Figure 6 evaluates analysis error variance as a function of observational information and the growth rate of error, assuming information from the FG and observations are combined with an optimal weight (w^*). As the estimation of the optimal weight is problematic (e.g., Houtekamer & Zhang, 2016), the weights used in real-life DA systems may be suboptimal. What is the effect of such weights on the quality of the analysis?

We assess how the use of suboptimal weight w affects analysis error variance in general. Figure 7 illustrates the relative change (in %) of analysis error variance a^2 compared to the optimal value (i.e., Figure 6 and Equation 16) as a function of error growth rate $e^{\alpha \cdot \Delta t}$. This is shown for cases where the corresponding weight w is over- (red line) or underestimated (blue line) by 20% relative to the optimal weight. This estimation is based on the analysis error equation in equilibrium (Equation 20), where the suboptimal weight w is set to be 20% larger or lower than

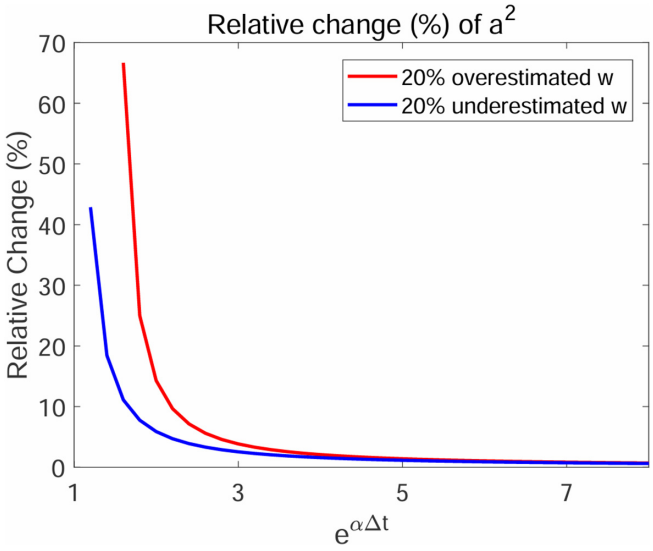

FIGURE 7 The relative change (%) of analysis error variance compared to the optimal value as a function of error growth rate $e^{\alpha \cdot \Delta t}$ when the corresponding weight w is (a) overestimated and (b) underestimated by 20% relative to the optimal weight.

the optimal weight (Equation 14). Due to the offset of o^2 in the calculation, the relative change of a^2 is independent of o^2 and only depends on $e^{\alpha \cdot \Delta t}$ and w.

Figure 7 demonstrates that both overestimation and underestimation of the weight w lead to increased analysis error variance compared to the optimal values. The relative increase in analysis error variance is strongly influenced by the error growth rate. Notably, the sensitivity of the analysis error variance to misestimation of w decreases as the error dynamics become more unstable. It is essentially due to the much-reduced weight on FG under strong instabilities (see Equation 14). Also, analysis error is more sensitive to the overestimation than the underestimation of w, that is, the asymmetry, which is further discussed in Figures 8 and 11.

In a more practical context, Figure 8 displays analysis error variance (a^2) and analysis information (I^a as defined in Equation 5b) as a function of the FG weight w and error growth rate $e^{\alpha \cdot \Delta t}$ in the form of a 3D plot (panel a) and a line graph (panel b), respectively, for a typical observational error variance $o^2 = 100\,m^2$ (i.e., the mean at the four operational centers in Table 2). Evident on both panels is the gradual decrease of analysis error variance as w approaches its optimal value from below, after which further increases in w lead to a more abrupt increase in analysis error. We return to the asymmetric increase of analysis error variance to under- versus overestimation of w^* in Section 4.2.2.

Another observation in Figure 8 as well as in Figure 7 is that error growth rate has an important influence on analysis error variance not only with optimal (Figure 6), but also with suboptimal weights. The more unstable a system is, the larger the analysis error variance, and the smaller the weight w^* an optimal analysis would use are (cf. high vs low growth rate situations in Figure 8b). The minimal analysis error variance values (a^{*2}) are highlighted with a dashed line on Figure 8.

6.2 | Application to operational systems

So far, we have presented a theoretically oriented analysis of two unmeasurable quantities, true error variance and

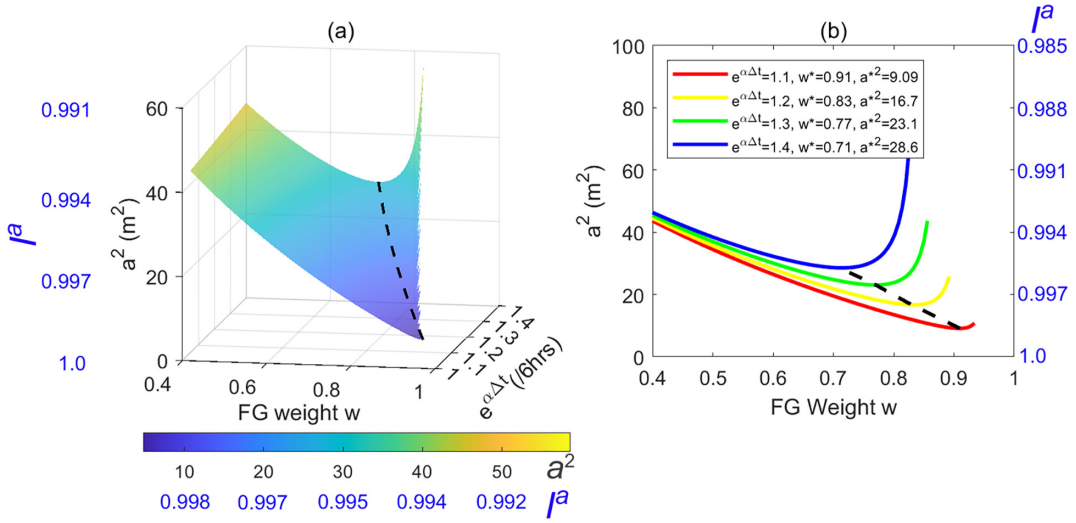

FIGURE 8 (a) Analysis error variance a^2 and information I^a as a function of the first-guess weight w and as a continuous (a) or discretized function of the error growth rate (b) $e^{\alpha \cdot \Delta t} = 1.1$ [red], 1.2 [yellow], 1.3 [green], and 1.4 [blue]), respectively, under $o^2 = 100\,m^2$. Black dashed lines indicate the optimal analysis error variance a^{*2}.

TABLE 3 Estimates of information in the first guess, observation, and analysis (with actual and optimal weights) states in the four operational DA systems.

Parameter/ center	Information in actual analysis	Information in first guess	Information in observation	Information in optimal analysis
Symbol	I^{a}	I^{f}	I^{o}	I^{a*}
NCEP	0.9986	0.9982	0.9945	0.9988
CMC	0.9989	0.9985	0.9963	0.9991
ECMWF	0.9996	0.9994	0.9990	0.9997
FNMOC	0.9981	0.9976	0.9928	0.9983

information in DA systems. As pointed out in Section 2, since the exact state of reality is unknown, the estimation of these quantities in the analysis, FG, or observations, however, is a challenging task. How can we apply these concepts in practice?

6.2.1 | Basic parameters

Peña and Toth (2014) proposed a method for the bias-free estimation of expected true error variance in numerical analysis and forecast fields called SAFE estimation (Feng *et al.*, 2017, 2020, 2023). SAFE assumes that in the short term, in a time-averaged sense, true error variance grows exponentially. The evolution of true error is then described by two parameters, analysis error variance (a^2) and the exponential error growth rate ($e^{\alpha \cdot \Delta t}$). These parameters, as well as a third independent quantity, the correlation between true error in the analysis and first guess (ρ), are then estimated using an inverse method. The method is based on the recognition that the expected behavior of perceived error can be simulated via the three unknown parameters (a^2, $e^{\alpha \cdot \Delta t}$, ρ), which are estimated by minimizing the residual difference between simulated and measured perceived error variance values.

Below we use analysis error variance and error growth rate estimates that Peña and Toth (2014) derived for 500-hPa height over the Northern Hemisphere extratropics (30–90° N) for DA systems used at four operational centers in 2008 (National Centers for Environmental Prediction – NCEP; Canadian Meteorological Center – CMC; European Center for Medium-range Weather Forecast – ECMWF; and Fleet Numerical Meteorology and Oceanography Center – FNMOC; see their Table 2).[v] Based on these estimates and on the triangle relationship in Figure 3, true error variance in the observation (o^2) and FG fields (f^2) and the effective weight w used on the FG (Equations 7 and 11) can also be calculated. Using estimates of the observational error variance (o^2) and growth rate ($e^{\alpha \cdot \Delta t}$), the optimal weight factor w^* and the error variance in an analysis made with the optimal weight (a^{*2}) can also be derived (Equation 16). Presented below are seven estimated parameters for the four DA systems studied here (Table 2), along with corresponding observational, FG, and analysis information derived through Equation (5b) (Table 3).

6.2.2 | Quality of optimal versus actual analyses

Analogous to Figures 6 and 9 color shades corresponding to the vertical axis measure the quality of analysis fields with optimal weights in terms of information (I^{a*}) and error variance (a^{*2}), as a function of growth rate (right axis) and observational error variance (left axis). Also shown in Figure 9 is the performance of 500-hPa height analysis fields in NH at the four operational data assimilation systems with actual weights (a^2 and I^{a}, closed circles), as well as analysis performance had optimal weights been used (a^{*2} and I^{a*} open circles, cf. Table 2). For comparability of data from simulations and the operational systems, Figure 9 uses non-standardized observational and analysis error variances in the range of the four DA systems.

First we note that of the four centers, the ECMWF DA system performs the best. The ECMWF analysis contains the highest level of information ($I^{a} = 0.9996$) and the lowest level of error variance (11.5 m^2), followed by CMC, NCEP, and FNMOC with 29.5, 38.0, and 49.2 m^2 error variance, respectively. This is consistent with the generally held notion that ECMWF forecast quality is superior to any other center's. A second observation in Figure 9 is that for all centers including ECMWF the points representing the actual analysis (closed circles) are above the surface of optimal analysis error. This indicates that the actual analyses are of noticeably poorer quality than an analysis made with the same amount of observational information but with optimal weights would be (open circles). Next, we assess how the actual analyses are affected by the use of suboptimal weights.

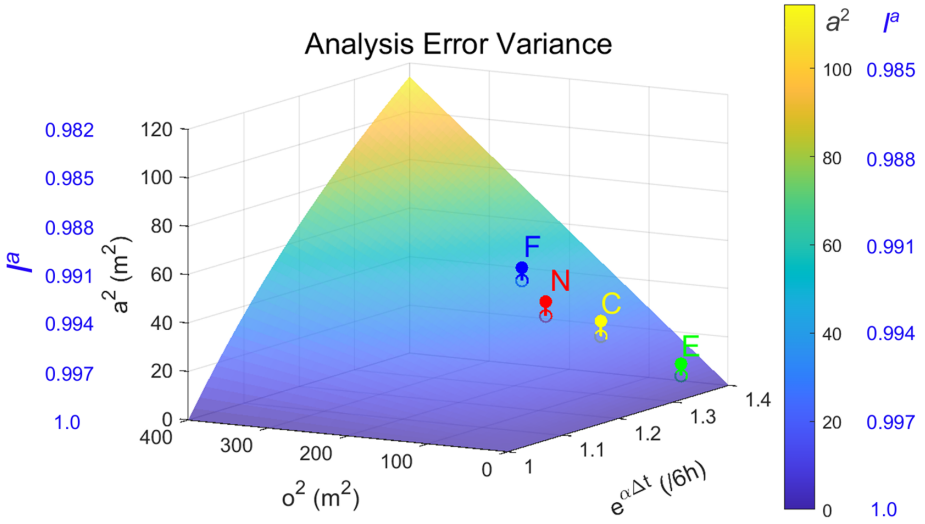

FIGURE 9 Same as Figure 6, except for a limited parameter space and using non-standardized error variance. Error variances and information in actual and optimized analyses from FNMOC (F), NCEP (N), CMC (C), and ECMWF (E) are shown by solid and open circles, respectively.

The geometric relations of states **A**, **F**, **O** in each operational DA system amongst themselves and with respect to **R** (see Figure 9) are qualitatively consistent with the schematic in Figure 3. Notably, in all four DA systems **A** is displaced toward **O** compared to the position of an analysis made with the same FG and observational information, but with an optimal weight ($\mathbf{A}^{*\prime}$). Lacking unbiased estimates of related error variances, the choice of the weights on the FG and observations involves a subjective consideration. Apparently, DA systems tend to underestimate the quality of the FG as in all four systems studied the diagnosed weight on the FG (w, see Table 2) is below the optimal value w^*, which, based on the mean of the estimated growth rates at the four centers ($e^{\alpha\cdot\Delta t} = 1.31$) is around 0.75 (Equation 14). This may be so as analysis error increases much more due to an over- than to an underestimate of w^* (see Figure 8). Obviously, erring on the positive side of w^* would disproportionately increase analysis error variance.

6.2.3 | Potential gain from optimal weights

How much information is lost, or error variance is added in each of the four analyses studied due to the use of lower than optimal weights? Displayed in Figure 11 are analysis error variance (a^2, Equation 20) and analysis information (I^a, Equation 23) as a function of the FG weight factor w and a continuous (panel a) and discrete function of observational error variance o^2 (panel b) for a growth rate close to that diagnosed for all four of the operational forecast systems studied ($e^{\alpha\cdot\Delta t} = 1.31$). The performance of each operational DA system is marked by a closed circle. Since for all systems error growth rate is near the prescribed value of $e^{\alpha\cdot\Delta t} = 1.31$, the closed circles are very close to the surface/lines on Figure 11a,b, respectively. As growth rate is fixed, analysis error variance associated with the optimal weight factor w^* (a^{*2}) fall on the straight lines in Figure 11a,b.

Apparently, as observational information (I^o) increases, analysis quality becomes less dependent on the weight chosen: the minimum at w^* on the curves in Figure 11b becomes progressively shallower. The fact that finding the minimum on shallower curves is harder may explain why error in the estimate of w increases as I^o increases from the smallest (FNMOC, top curve in Figure 11b) to the largest value (ECMWF, bottom curve).

Interestingly, the absolute loss of information, or the accrual of error variance due to the use of suboptimal weights is rather similar at the four centers, the latter in the range of 4.9–6.3 m^2. This, given the similarity of the four curves in Figure 11b, corresponds with an orderly increase of additive bias in the estimate of w^* from a modest 0.09 at the lowest-performing (FNMOC), to a more severe 0.34 at the best-performing center (ECMWF). One might speculate that the similarity of error in the estimate of w may reflect a limitation linked with uncertainty in other DA parameters, shared by all four centers.

Could optimal weights be integrated into practical DA systems, and if so, how much improvement might they deliver in operational analyses and forecasts? As demonstrated above, both w and w^* can be directly estimated for operational systems using SAFE and the methodology developed in this study. Optimization is achieved by applying the scalar ratio w^*/w to the FG weight and its inverse to the weights on individual observation types. To illustrate, we evaluate the impact of optimal weights on the four systems discussed above (Table 2). Improvements expected from the first introduction of w^* are shown in Figure 10 (cf. a^2 vs. $a^{*\prime 2}$). Assuming observational information and

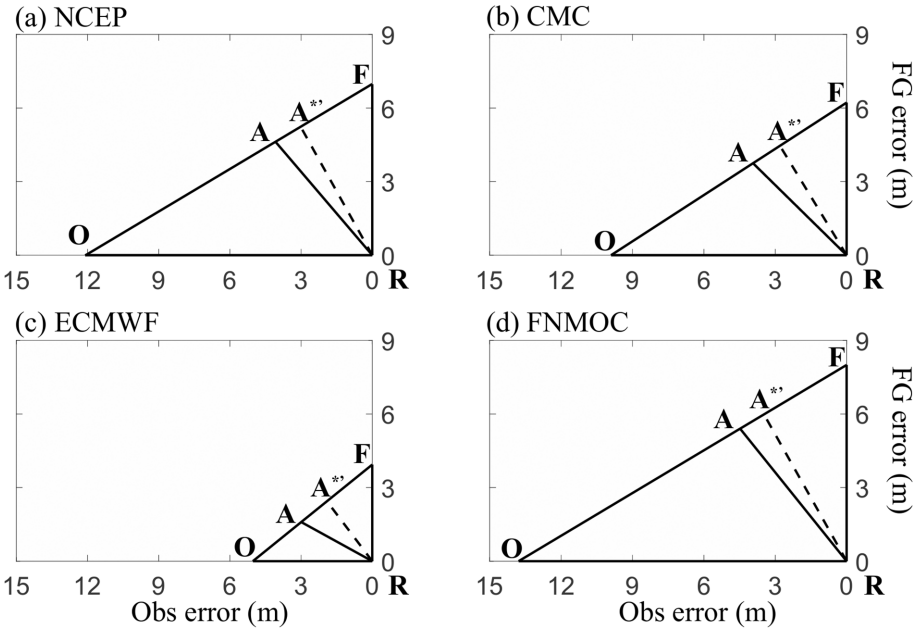

FIGURE 10 Same as the schematic in Figure 3, except based on parameters estimated from four operational DA systems: (a) NCEP, (b) CMC, (c) ECMWF, and (d) FNMOC. See text for further details.

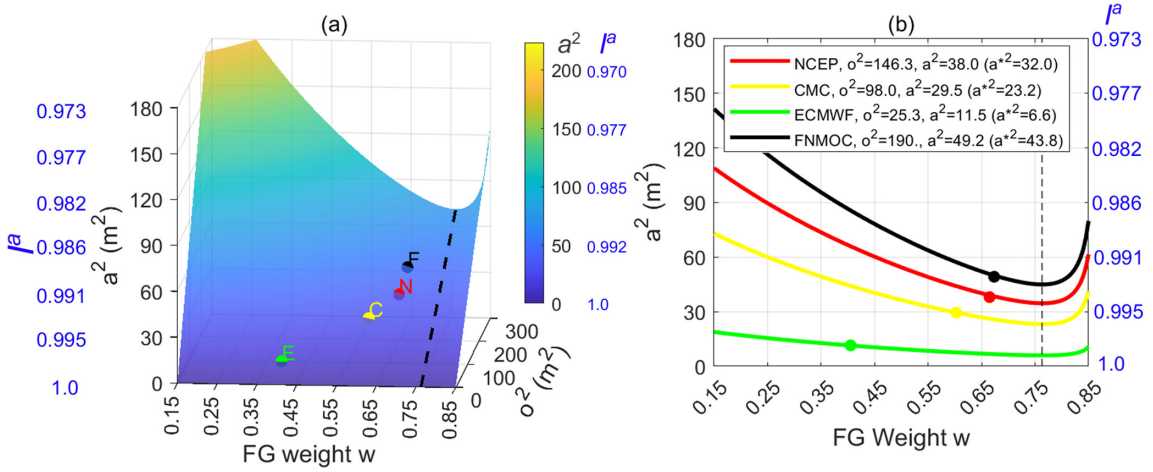

FIGURE 11 (a) Variation of a^2 as a function of w and a continuous (panel a) and discrete function of o^2 (b, for $o^2 = 146.3$, 98.0, 25.3, and 190.0 m^2 for the operational DA systems at NCEP (red, N), CMC (yellow, C), ECMWF (green, E), and FNMOC (black, F), respectively), with $e^{\alpha \cdot \Delta t} = 1.31$. Values of a^2 for the four systems are marked by solid circles. Black dashed lines indicate the optimal analysis error variance a^{*2}.

error growth rates remain stationary, further gains are expected in subsequent cycles. Because w^* reduces analysis error, the associated FG error also declines, leading to a progressive reduction in both analysis and FG errors (see Section 5.5). The process converges at a^{*2}, the error variance corresponding to optimal weights. This convergence mirrors the evolution of an analysis cycle initiated with an FG error exceeding its expected value (see Section 5.5 and panel a in Figure A1 in the Appendix).

Adjusting global weight factors of observation and FG to their optimal values reduces analysis error variance by 11%–43% across the four centers (Table 2). We must point out, however, that w^*/w was estimated over the same three-month period used for the evaluation of its effect, and hence the estimate is subject to overfitting error. Independent sample-based estimates are likely to lead to somewhat smaller improvements in analysis performance due to relatively small changes in the observing network and error growth regimes. If enough data are available, weights, on the other hand, can also be statistically optimized by region, model level, and/or observation types, which could provide further potential improvements. Note that with the use of hybrid covariances, several centers

already condition their weights on ensemble-based, case-to-case estimates of error growth rate (e.g., Wang *et al.*, 2013).

6.2.4 | What drives analysis quality?

As we saw in Section 4.2.3, the use of suboptimal weights equally affects the quality of analyses at all four centers. What drives then the difference of nearly a factor of four observed in the quality of analyses at the different centers? Is it forecast quality, or observational information? Obviously, forecast quality is contingent on the fidelity of numerical models used. Since the growth rates of short-range forecast error are very similar at the four centers (around 1.31 per 6 h, Table 2), analysis accuracy must primarily (and for $\mathbf{A}^*$, exclusively) reflect information extracted from the observations (or error variance in the hypothetical observation field, cf. Tables 2 and 3). It follows that analysis quality is primarily driven not by error in a model FG forecast (Step 1), or by the weight factor w (Step 4), but by the information extracted from the mostly same set of observations shared among all operational centers. So it is Steps 2 and 3 of DA systems (i.e., observational and forward operators, background covariances and related procedures, Section 3.3) that appear to be the critical, distinguishing factors in terms of the quality and performance of analysis and short-range forecast systems.

7 | CONCLUSIONS AND DISCUSSION

Factors affecting current forecast skill, and potential limitations to future improvements due to limited atmospheric predictability have been studied extensively. A theoretical analysis of limitations in environmental monitoring of natural systems, or assessing the current state of the atmosphere, on the other hand, have received less attention. Under certain conditions, information about the state of a natural system extracted from observations may synchronize the behavior of an abstract replica with its target. What controls the level of synchronization if a realistic numerical model of the natural system is available? In this study we identified a few basic parameters that quantitatively control the amount of information we can assess about the state of chaotic systems in nature.

To monitor the evolution of a natural system, observing systems continuously collect measurements about its condition. No matter how extensive they are, observations at any point in time provide only limited information about the state of a system. If the dynamics of a deterministic system is known, information from past observations, however, can be propagated to the current time. On the coarser, resolved scales and in an abstract form, numerical models capture the dynamical evolution of prognostic variables of the real atmosphere. In data assimilation, short range first-guess forecasts from such models (**F**), starting from a previous estimate of the state are used in a recursive manner to carry observational information extracted from past observations to the current time. Recent observations are interpreted in terms of the model prognostic variables (hypothetical observational field, **O**).

Conceptually, an analysis (**A**) can be considered as a weighted sum of the FG forecast (with a weight of w), containing information extracted from all past observations that is retained through the periodic use of forecasts in cycled DA systems, and the observational field containing all information extracted from the most recent set of measurements (with a weight of $1 - w$). Such an analysis is an abstract representation of key aspects of the state of a natural system (**T**) that a monitoring system can resolve. Considering the anomalies of **T**, and of its estimates **O**, **F**, and **A** from the climatic mean of the natural system, the anomaly variance in the estimates identical to the realization of anomaly variance in **T** we call information. For forecast systems with no bias and realistic variance, information in an anomaly field is directly related to the growing part of error associated with that field (Equations 5a and 5b).

The performance of data assimilation systems (measured here by information in the analysis, I^a) was found to be controlled just by two or three parameters: the amount of observational information they extract from the latest set of observations (I^o), the chaotic loss of information due to error growth ($e^{\alpha \cdot \Delta t}$), and if suboptimal, the weight on the FG (w). The second, error growth parameter ($e^{\alpha \cdot \Delta t}$) reflects the "agility" of the natural system, and is related to the rate of divergence of initially similar segments of the system's trajectory. The first parameter (I^o) reflects the rate at which new information about the natural system is accessed in time, relative to the total amount of information needed to perfectly define the state of a system at a given resolution (which equals 1). This is influenced by the number and quality of measurements the observing system provides, and how much information is extracted and used from them by the DA system. The third parameter (w) is a sole function of the DA system.

A key recognition of this study is that in a statistical sense, observational information entered into an analysis from the latest measurements equals the loss of

information endured by the FG used in the analysis. In other words, in DA cycles with stationary performance there is an equivalence between observational gain and the forecast loss of information. Pursuant of this equilibrium, simulations with the key parameters reveal the general conditions necessary for the successful monitoring of natural systems. This may be helpful, for example, in preparation for the monitoring of newly explored systems such as the atmosphere of other planets, before the deployment of any observing systems there. As for the influence of past observations, most (more than 99% of) information in an analysis is found to originate from observations in the most recent 72 hours. This suggests that 4DVar assimilation windows may not need to extend into the past beyond this time window.

Since a method for the bias-free estimation of analysis error variance and forecast error growth (or information loss) is available (SAFE, Peña & Toth, 2014), observational information extracted by real-world DA applications (I^o) can, for the first time, also be quantified. Of the four weather forecast systems operational in 2008 studied, ECMWF, long recognized as the best-performing center, was found to extract the highest amount of standardized information from the approximately same volume of observations used by all systems, resulting in a 500-hPa height analysis error variance of 11.5 m^2 (Table 2). CMC, NCEP, and FNMOC were found to extract less information from observations and exhibit higher analysis error variances of 29.5, 38.0, and 49.2 m^2, respectively. An application to more recent data may unveil operationally relevant diagnostic information about the current performance of NWP systems. Future extensions of the method may also quantify observational information extracted from different types of observational instruments and platforms.

Traditionally, in DA schemes estimated error covariances control the general parameter of the relative weight on observations and the FG. A theoretical analysis, however, indicates that the optimal ratio between the weight on the FG (w^*) versus observations ($1 - w^*$) depends only on the growth rate of error (Equation 14). As error variance estimates may contain biases, it is not surprising that all four centers are found to use suboptimal weights on the FG and observations. Moreover, the weight on the FG (w) is underestimated at all centers (Table 2). This may not be a coincidence since as indicated by our simulations, analysis error variance would increase much steeper had w been overestimated (Figure 10). The largest/smallest error in w is observed at ECMWF/FNMOC. This is also understandable since the minimum in analysis error variance as w changes becomes shallower and harder to find as analysis performance improves.

The theoretical identification of the optimal weights may have significant practical implications. A simple adjustment of the relative weights on observations versus the FG in the four 2008 systems is estimated to yield up to an 11%–43% reduction in analysis error variance at the four centers. As for the key parameter controlling the quality of analyses, since the growth rate of forecast error is similar at the four centers (around 1.31 per six hours), differences in analysis performance are primarily driven not by model performance or the choice of w, but by the amount of information used from the latest set of observations (I^o).

Though there is a considerable amount of theory that supports DA algorithms, operational systems emerged and have evolved over time in an organic, somewhat ad-hoc manner. None of the systems, for example, produce a purely observationally based field (**O**) referenced in the diagnostic approach above. The simple conceptual description of DA through **O**, **F**, and w, and the recognition of the equivalence between the loss of forecast information due to limited atmospheric predictability, and the gain of information from the most recent batch of observations offer some new, quantitative insights into the limits of assessing the state of chaotic systems in nature. As another practical implication, DA systems could perhaps be simplified along the conceptual lines highlighted above. Such a redesign may yield easier to diagnose and tune systems that may therefore be more amenable to optimization and further development.

ACKNOWLEDGEMENTS

The research reported here was carried out while the first author held a National Research Council Associateship at the Global Systems Laboratory (GSL) of the National Oceanic and Atmospheric Administration. The support of Jennifer Mahoney, Dr. Curtis Alexander, and Kevin Kelleher, current Director and Deputy Director, and former Director of GSL, respectively, are gratefully acknowledged. The first author was partially supported by the National Natural Science Foundation of China (Grant No. 42375058).

FUNDING INFORMATION

The first author was partially supported by the National Natural Science Foundation of China (Grant No. 42375058).

DATA AVAILABILITY STATEMENT

The data that support the findings of this study are available from the corresponding author upon reasonable request.

ENDNOTES

[i] For some applications, numerical models may include some stochastic components (Buizza *et al.* 1999; Leutbecher *et al.* 2017).

[ii] Note that since it has not been presented before, existing DA applications do not follow this conceptual framework. For example, as further discussed below, DA schemes do not create an observational field, and use observational type-dependent weighting factors. In practice, the weighting factor is a high-dimensional matrix that varies both spatially and temporally. To reduce the complexity of the error behavior model to be introduced next, and to better isolate the fundamental mechanisms that influence analysis quality, the scalar w in Equation (6) reflects the global average weights on the FG.

[iii] Figure 3, drawn in the model's space is analogous to Figure 1 of Desroziers *et al.* (2005) drawn in the space of individual observation types, except we omit their implicit assumption that in practical data assimilation applications observational and background error variances are perfectly estimated.

[iv] As mentioned in Section 3.3, DA applications do not explicitly create an observational field. Instead, they employ multiple weights for different observation types. Notably, as will be demonstrated in Section 4.2.1, the ratio in Equation (15) can still be directly quantified for real-world DA systems.

[v] The application here is for demonstration purposes. True error variance data from Peña and Toth (2014) are used for convenience as the availability of these statistics makes the calculation of the diagnostics proposed here trivial.

ORCID

Jie Feng https://orcid.org/0000-0002-2480-2003

REFERENCES

Albers, S., Saleeby, S.M., Kreidenweis, S., Bian, Q., Xian, P., Toth, Z. et al. (2020) A fast visible-wavelength 3D radiative transfer model for numerical weather prediction visualization and forward modeling. *Atmospheric Measurement Techniques*, 13(6), 3235–3261. Available from: https://doi.org/10.5194/amt-13-3235-2020

Anderson, J.L. (2001) An ensemble adjustment Kalman filter for data assimilation. *Monthly Weather Review*, 129, 2884–2903. Available from: https://doi.org/10.1175/1520-0493(2001)129,2884:AEAKFF.2.0.CO;2

Bannister, R.N. (2008) A review of forecast error covariance statistics in atmospheric variational data assimilation. I: characteristics and measurements of forecast error covariances. *Quarterly Journal of the Royal Meteorological Society*, 134, 1951–1970. Available from: https://doi.org/10.1002/qj.339

Bannister, R.N. (2017) A review of operational methods of variational and ensemble-variational data assimilation. *Quarterly Journal of the Royal Meteorological Society*, 143, 607–633. Available from: https://doi.org/10.1002/qj.2982

Bauer, P., Thorpe, A. & Brunet, G. (2015) The quiet revolution of numerical weather prediction. *Nature*, 525, 47–55. Available from: https://doi.org/10.1038/nature14956

Bechtold, P., Köhler, M., Jung, T., Doblas-Reyes, F., Leutbecher, M., Rodwell, M.J. et al. (2008) Advances in simulating atmospheric variability with the ECMWF model: from synoptic to decadal time-scales. *Quarterly Journal of the Royal Meteorological Society*, 134(634 A), 1337–1351. Available from: https://doi.org/10.1002/qj.289

Bengtsson, T., Bickel, P. & Li, B. (2008) Curse-of-dimensionality revisited: collapse of the particle filter in very large scale systems. In: *Probability and statistics: essays in honor of David a. freedman, D. Nolan and T. Speed*, Vol. 2. Beachwood, OH: Institute of Mathematical Statistics, pp. 316–334.

Bertino, L., Evensen, G. & Wackernagel, H. (2003) Sequential data assimilation techniques in oceanography. *International Statistical Review*, 71, 223–241.

Bouttier, F. (2001) *The development of 12-hourly 4D-Var*. Reading, UK: ECMWF. Technical Memorandum, Vol. 348.

Bouttier, F. & Courtier, P. (2002) Data assimilation concepts and methods March 1999. Training, (March 1999), 59. http://www.mendeley.com/research/data-assimilation-concepts-and-methods/

Buizza, R., Milleer, M., & Palmer, T. N. (1999) Stochastic representation of model uncertainties in the ECMWF ensemble prediction system. *Quarterly Journal of the Royal Meteorological Society*, 125, 2887–2908.

Cao, Y., Zhu, J., Navon, I.M. & Luo, Z. (2007) A reduced order approach to four dimensional variational data assimilation using proper orthogonal decomposition. *International Journal for Numerical Methods in Fluids*, 53, 1571–1583.

Carrassi, A., Bocquet, M., Bertino, L. & Evensen, G. (2018) Data assimilation in the geosciences: an overview of methods, issues, and perspectives. *WIREs Climate Change*, 9, e535. Available from: https://doi.org/10.1002/wcc.535

Charney, J.G. (1948) On the scale of atmospheric motion. *Geofysiske Publikasjoner*, 17, 1–17.

Charney, J.G., Fjörtoft, R. & Von Neumann, J. (1950) Numerical integration of the Barotropic vorticity equation. *Tellus Series A: Dynamic Meteorology and Oceanography*, 2(4), 237–254. Available from: https://doi.org/10.3402/tellusa.v2i4.8607

Courtier, P., Thepaut, J.-N. & Hollingsworth, A. (1994) A strategy for operational implementation of 4D-Var, using an incremental approach. *Quarterly Journal of the Royal Meteorological Society*, 120, 1367–1387.

Crisan, D. & Ghil, M. (2023) Asymptotic behavior of the forecast-assimilation process with unstable dynamics. *Chaos*, 33(2), 023139. Available from: https://doi.org/10.1063/5.0105590

Daley, R. (1991) *Atmospheric data analysis*. Cambridge, UK: Cambridge University Press, p. 457.

De Rosnay, P., Browne, P., De Boisséson, E. et al. (2022) Coupled data assimilation at ECMWF: status, challenges, and future developments. *Quarterly Journal of the Royal Meteorological Society*, 148, 2672–2702. Available from: https://doi.org/10.1002/qj.4330

Desroziers, G., Berre, L., Chapnik, B. & Poli, P. (2005) Diagnosis of observation, background and analysis-error statistics in observation space. *Quarterly Journal of the Royal Meteorological Society*, 131, 3385–3396.

Feng, J., Li, J.P., Zhang, J., Liu, D.Q. & Ding, R.Q. (2019) The relationship between deterministic and ensemble mean forecast errors revealed by global and local attractor radii. *Advances in Atmospheric Sciences*, 36(3), 271–278.

Feng, J., Toth, Z. & Peña, M. (2017) Spatial extended estimates of analysis and short-range forecast error variances. *Tellus A*, 69(1), 1325301. Available from: https://doi.org/10.1080/16000870.2017.1325301

Feng, J., Toth, Z. & Pena, M. (2020) Partition of analysis and forecast error variance into growing and decaying components. *Quarterly Journal of the Royal Meteorological Society*, 146(728), 1302–1321.

Feng, J., Toth, Z., Zhang, J. & Pena, M. (2024) Ensemble forecasting: a foray of dynamics into the realm of statistics. *Quarterly Journal of the Royal Meteorological Society*, 150(762), 2537–2560. Available from: https://doi.org/10.1002/qj.4745

Feng, J., Wang, J., Dai, G., Zhou, F. & Duan, W. (2023) Spatiotemporal estimation of analysis errors in the operational global data assimilation system at the China Meteorological Administration using a modified SAFE method. *Quarterly Journal of the Royal Meteorological Society*, 149, 230. Available from: https://doi.org/10.1002/qj.4507

Hamill, T., Snyder, M.C. & Morss, R.E. (2002) Analysis-error statistics of a quasi-geostrophic model using three-dimensional variational assimilation. *Monthly Weather Review*, 130, 2777–2791.

Harris, L., Zhou, L., Lin, S.J., Chen, J.H., Chen, X., Gao, K. et al. (2020) GFDL SHiELD: a unified system for weather-to-seasonal prediction. *Journal of Advances in Modeling Earth Systems*, 12(10), e2020MS002223. Available from: https://doi.org/10.1029/2020MS002223

Holton, J.R. & Hakim, G.J. (2012) An introduction to dynamic meteorology. In: *An introduction to dynamic meteorology*, 5th edition. Singapore: Academic Press, pp. 1–532. Available from: https://doi.org/10.1016/C2009-0-63394-8

Houtekamer, P.L. & Zhang, F. (2016) Review of the ensemble Kalman filter for atmospheric data assimilation. *Monthly Weather Review*, 144, 4489–4532. Available from: https://doi.org/10.1175/MWR-D-15-0440.1

Hunt, B.R., Kostelich, E. & Szunyogh, I. (2007) Efficient data assimilation for spatiotemporal chaos: a local ensemble transform Kalman filter. *Physica D: Nonlinear Phenomena*, 230, 112–126. Available from: https://doi.org/10.1016/j.physd.2006.11.008

Ide, K., Courtier, P., Ghil, M. & Lorenc, A.C. (1997) Unified notation for data assimilation: operational, sequential, and variational. *Journal of the Meteorological Society of Japan*, 75B, 181–189.

Janjić, T., Bormann, N., Bocquet, M., Carton, J.A., Cohn, S.E., Dance, S.L. et al. (2018) On the representation error in data assimilation. *Quarterly Journal of the Royal Meteorological Society*, 144(713), 1257–1278. Available from: https://doi.org/10.1002/qj.3130

Kalnay, E. (2003) *Atmospheric modeling, data assimilation and predictability*. Cambridge, UK: Cambridge University Press, pp. 175–184.

Kumar, A., Kim, H. & Hancke, G.P. (2013) Environmental monitoring systems: a review. *IEEE Sensors Journal*, 13(4), 1329–1339. Available from: https://doi.org/10.1109/JSEN.2012.2233469

Lazo, J.K., Morss, R.E. & Demuth, J.L. (2009) 300 billion served - sources, perceptions, uses, and values of weather forecasts. *Bulletin of the American Meteorological Society*, 90(6), 785–798.

Lei, L. & Whitaker, J.S. (2017) Evaluating the trade-offs between ensemble size and ensemble resolution. *Journal of Advances in Modeling Earth Systems*, 9, 781–789.

Leith, C.E. (1974) Theoretical skill of Monte Carlo forecasts. *Monthly Weather Review*, 102(6), 409–418.

Leutbecher, M., Lock, S. J., Ollinaho, P., Lang, S. T., Balsamo, G., Bechtold, P. et al. (2017) Stochastic representations of model uncertainties at ECMWF: State of the art and future vision. *Quarterly Journal of the Royal Meteorological Society*, 143(707), 2315–2339.

Li, J.P. & Ding, R.Q. (2011) Temporal–spatial distribution of atmospheric predictability limit by local dynamical analogues. *Monthly Weather Review*, 139, 3265–3283.

Li, J.P., Ding, R.Q. & Chen, B.H. (2006) Review and prospect on the predictability study of the atmosphere (in Chinese). In: *Review and prospects of the developments of atmosphere sciences in early 21st century*. Beijing, People's Republic of China: China Meteorology Press, pp. 96–104.

Li, J.P., Feng, J. & Ding, R.Q. (2018) Attractor radius and global attractor radius and their application to the quantification of predictability limits. *Climate Dynamics*, 51, 2359–2374. Available from: https://doi.org/10.1007/s00382-017-4017-y

Lorenc, A.C. (1986) Analysis methods for numerical weather prediction. *Quarterly Journal of the Royal Meteorological Society*, 112(474), 1177–1194. Available from: https://doi.org/10.1002/qj.49711247414

Lorenc, A.C. (2003) The potential of the ensemble Kalman filter for NWP: a comparison with 4D-var. *Quarterly Journal of the Royal Meteorological Society*, 129, 3183–3203. Available from: https://doi.org/10.1256/qj.02.132

Lorenz, E.N. (1963) Deterministic nonperiodic flow. *Journal of the Atmospheric Sciences*, 20, 130–141.

Lorenz, E.N. (1969) The predictability of a flow which possesses many scales of motion. *Tellus A: Dynamic Meteorology and Oceanography*, 21(3), 289. Available from: https://doi.org/10.3402/tellusa.v21i3.10086

Marshall, J. & Molteni, F. (1993) Towards a dynamical understanding of planetary-scale flow regimes. *Journal of the Atmospheric Sciences*, 50, 1792–1818.

Palmer, T.N. (2012) Towards the probabilistic earth-system simulator: a vision for the future of climate and weather prediction. *Quarterly Journal of the Royal Meteorological Society*, 138(665), 841–861. Available from: https://doi.org/10.1002/qj.1923

Patil, D.J., Hunt, B.R., Kanlay, E., Yorke, J.A. & Ott, E. (2001) Local low–dimensionality of atmospheric dynamics. *Physical Review Letters*, 86, 5878–5881.

Peña, M. & Toth, Z. (2014) Estimation of analysis and forecast error variances. *Tellus*, 66, 21767. Available from: https://doi.org/10.3402/tellusa.v66.21767

Pires, C., Vautard, R. & Talagrand, O. (1996) On extending the limits of variational assimilation in nonlinear chaotic systems. *Tellus, Series A: Dynamic Meteorology and Oceanography*, 48(1), 96–121.

Privé, N. & Errico, R.M. (2013) The role of model and initial condition error in numerical weather forecasting investigated with an observing system simulation experiment. *Tellus A: Dynamic Meteorology and Oceanography*, 65, 21740. Available from: https://doi.org/10.3402/tellusa.v65i0.21740

Raynaud, L., Berre, L. & Desroziers, G. (2011) Accounting for model error in the Meteo-France ensembledata assimilation system. *Quarterly Journal of the Royal Meteorological Society*, 138, 249–262. Available from: https://doi.org/10.1002/qj.906

Reichle, R.H. (2008) Data assimilation methods in the earth sciences. *Advances in Water Resources*, 31(11), 1411–1418. Available from: https://doi.org/10.1016/j.advwatres.2008.01.001

Richardson, L.F. (1922) *Weather prediction by numerical process*. Cambridge, UK: Cambridge University Press, p. 236.

Schultz, M.G., Betancourt, C., Gong, B., Kleinert, F., Langguth, M., Leufen, L.H. et al. (2021) Can deep learning beat numerical weather prediction? *Philosophical Transactions of the Royal Society A: Mathematical, Physical and Engineering Sciences*, 379, 20200097. Available from: https://doi.org/10.1098/rsta.2020.0097

Simmons, A.J. & Hollingsworth, A. (2002) Some aspects of the improvement in skill of numerical weather prediction. *Quarterly Journal of the Royal Meteorological Society*, 128(580), 647–677. Available from: https://doi.org/10.1256/003590002321042135

Sun, Y.Q. & Zhang, F. (2016) Intrinsic versus practical limits of atmospheric predictability and the significance of the butterfly effect. *Journal of the Atmospheric Sciences*, 73(3), 1419–1438. Available from: https://doi.org/10.1175/JAS-D-15-0142.1

Tondeur, M., Carrassi, A., Vannitsem, S. & Bocquet, M. (2020) On temporal scale separation in coupled data assimilation with the ensemble Kalman filter. *Journal of Statistical Physics*, 179(5–6), 1161–1185. Available from: https://doi.org/10.1007/s10955-020-02525-z

Toth, Z. & Buizza, R. (2018) Weather forecasting: what sets the forecast skill horizon? In: *Sub-seasonal to seasonal prediction: the gap between weather and climate forecasting*. Amsterdam, Netherlands: Elsevier, pp. 17–45. Available from: https://doi.org/10.1016/B978-0-12-811714-9.00002-4

Toth, Z. & Kalnay, E. (1997) Ensemble forecasting at NCEP: the breeding method. *Monthly Weather Review*, 125, 3297–3318.

Toth, Z., Talagrand, O. & Zhu, Y. (2006) The attributes of forecast systems: a general framework for the evaluation and calibration of weather forecasts. In: *Predictability of weather and climate*. Cambridge, UK: Cambridge University Press, pp. 584–595. Available from: https://doi.org/10.1017/CBO9780511617652.023

Wang, L., Liu, Y., Xu, D., Zhang, L., Leung, J.C.H., Li, H. et al. (2024) An incremental analysis update in the framework of the four-dimensional variational data assimilation: description and preliminary tests in the operational China Meteorological Administration global forecast system. *Quarterly Journal of the Royal Meteorological Society*, 150(761), 2104–2122. Available from: https://doi.org/10.1002/qj.4699

Wang, X., Barker, D.M., Snyder, C. & Hamill, T.M. (2008a) A hybrid ETKF–3DVAR data assimilation scheme for the WRF model. Part I: observing system simulation experiment. *Monthly Weather Review*, 136, 5116–5131. Available from: https://doi.org/10.1175/2008MWR2444.1

Wang, X., Barker, D.M., Snyder, C. & Hamill, T.M. (2008b) A hybrid ETKF-3DVAR data assimilation scheme for the WRF model. Part II: real observing experiments. *Monthly Weather Review*, 136(12), 5132–5147. Available from: https://doi.org/10.1175/2008MWR2445.1

Wang, X., Parrish, D., Kleist, D. & Whitaker, J. (2013) GSI 3Dvar-based ensemble-variational hybrid data assimilation for NCEP global forecast system: single-resolution experiments. *Monthly Weather Review*, 141(11), 4098–4117.

Zhang, F., Qiang Sun, Y., Magnusson, L., Buizza, R., Lin, S.J., Chen, J.H. et al. (2019) What is the predictability limit of midlatitude weather? *Journal of the Atmospheric Sciences*, 76(4), 1077–1091. Available from: https://doi.org/10.1175/JAS-D-18-0269.1

Zupanski, D., Hou, A.Y., Zhang, S.Q., Zupanski, M., Kummerow, C.D. & Cheung, S.H. (2007) Applications of information theory in ensemble data assimilation. *Quarterly Journal of the Royal Meteorological Society*, 133(627), 1533–1545. Available from: https://doi.org/10.1002/qj.123

How to cite this article: Feng, J., Toth, Z. & Peña, M. (2026) The limits of knowing: An equilibrium between the observational gain and chaotic loss of information in data assimilation. *Quarterly Journal of the Royal Meteorological Society*, 152:e70067. Available from: https://doi.org/10.1002/qj.70067

APPENDIX A

A.1 Transitional behavior

In an expected sense, error variance in an analysis cycle undergoes a cyclic behavior: an instantaneous drop in error variance at the time of an observational update (Equation 19), followed by an exponential growth of error in the forecast phase (Equation 7). The fluctuating level of expected error variance (which is an inverse measure of information) observed in the unstable subspace of successive data assimilation cycles (that we assume use optimal weights based on bias-free error variance estimates) is graphically demonstrated on the right-hand side of each panel in Figure A1. The rest of Figure A1 explores what happens when an analysis cycle is started with an error in the first guess different from its expected value (Equation 16).

The most important observation in Figure A1 is that in a wide range of the parameter space, irrespective of the value of the error in the initial first guess, after a transitionary period, standardized analysis (a^{*2}) and first-guess error variances (f^2) asymptote to their expected value (Equation 16). As seen from the different experiments reported in Figure A1 and is also expected from Equation (16), the rate of convergence is a strong function of error growth. When $e^{\alpha \cdot \Delta t}$ increases from 1.31 (Figure A1a,b) to 4 per six hours (Figure A1c,d), analysis error variance approaches its saturation value in 2–6 (instead of 14–23) cycles. The effect of similar-magnitude changes in observational information is generally less dramatic (cf. blue and red vertical dashed lines in the various panels).

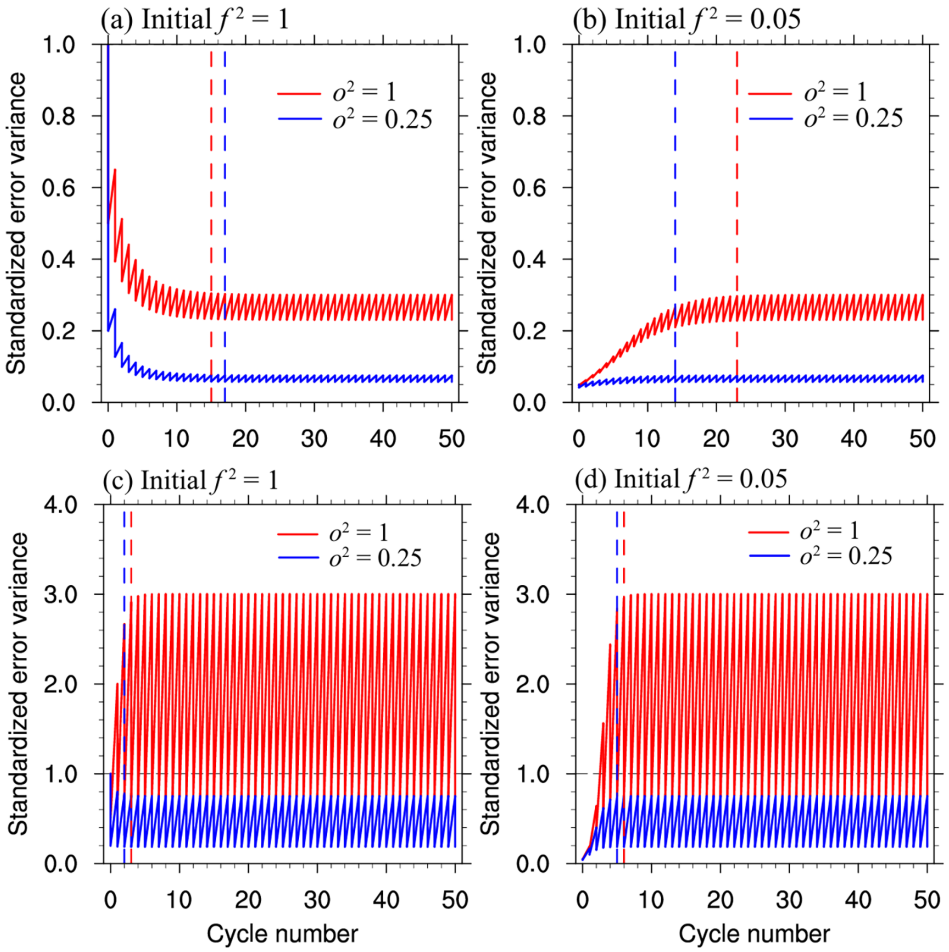

FIGURE A1 Variation of the standardized analysis (a^{*2}) and first-guess (f^2) error variances with the number of the assimilation-forecast cycle given the initial first-guess error variance $f^2 = 1$ (a,c) and $f^2 = 0.05$ (b,d). The standardized observational error variance is $o^2 = 1$ (red solid line) and 0.25 (blue solid line), while the error growth rate $e^{\alpha \cdot \Delta t}$ is 1.31 (panels a,b) and 4 per six hours (panels c,d). For each experiment, the dashed vertical line indicates the number of cycles after which analysis error variance reaches 99.9% of its saturation value. [Colour figure can be viewed at wileyonlinelibrary.com]